Stochastic Dynamics of Nanoparticle and Virus Uptake

Felix Frey, Falko Ziebert, and Ulrich S. Schwarz
Institute for Theoretical Physics, Heidelberg University, Philosophenweg 19, 69120 Heidelberg, Germany
and BioQuant, Heidelberg University, Im Neuenheimer Feld 267, 69120 Heidelberg, Germany

(Received 25 May 2018; revised manuscript received 6 December 2018; published 26 February 2019)

The cellular uptake of nanoparticles or viruses requires that the gain of adhesion energy overcomes the cost of plasma membrane bending. It is well known that this leads to a minimal particle size for uptake. Using a simple deterministic theory for this process, we first show that, for the same radius and volume, cylindrical particles should be taken up faster than spherical particles, both for normal and parallel orientations. We then address stochastic effects, which are expected to be relevant due to small system size, and show that, now, spherical particles can have a faster uptake because the mean first passage time profits from the multiplicative noise induced by the spherical geometry. We conclude that stochastic effects are strongly geometry dependent and may favor spherical shapes during adhesion-driven particle uptake.

DOI: 10.1103/PhysRevLett.122.088102

Biological cells constantly communicate with their environment by relaying signals and material across their plasma membranes. In particular, cells routinely take up small particles with sizes on the order of 10–300 nm. This process is usually driven by receptor-ligand interactions [1] such that the adhesion energy can overcome the energy required for membrane bending. It is also exploited by viruses that have to enter host cells for replication [2]. Due to the physical nature of this process, cells also take up artificial nanoparticles of various shapes [3], for which the uptake may be either intentional or undesired, as in drug delivery [4] or in the case of microplastics [5], respectively.

Viruses come in many different shapes [6], but the most paradigmatic and most frequently occurring ones are spherical and cylindrical [7,8]. Therefore, here, we focus our discussion on spheres, cylinders, and a combination of both, as shown in Fig. 1. It is generally believed that the spherical shape is optimal because it maximizes the volume to surface ratio and confers high mechanical stability [9]. However, it is less clear which shapes are optimal in regard to interactions with the membrane [3]. Here, we show that stochasticity might play an important role in this context.

Due to their small size, viruses are typically covered with only a few tens of ligands for cell surface receptors [10,11], and thus stochastic effects are expected to be relevant. For example, the icosahedral and medium-sized (60–100 nm) members of the family of reoviruses have only 12 primary JAM-A-σ1 (junction adhesion molecule) ligands on their surfaces [12]. Although stochastic effects have been argued to be essential for the stability of small adhesion clusters [13,14], particle uptake is usually studied analytically only with deterministic approaches. Stochastic effects are automatically included in computer simulations with thermostats [15,16], but such approaches do not allow for a systematic study of the role of noise. Here, we analytically calculate the first passage times for particle uptake of various shapes and show that they strongly depend on geometry. Our main result is that, in contrast to deterministic dynamics, stochastic dynamics tends to favor spherical shapes for uptake.

Deterministic approaches usually start by balancing the contributions from adhesion and bending. Because adhesion energy scales with the radius squared, while bending energy is independent of radius, a minimal size exists for particle uptake [17]. The most investigated aspect of

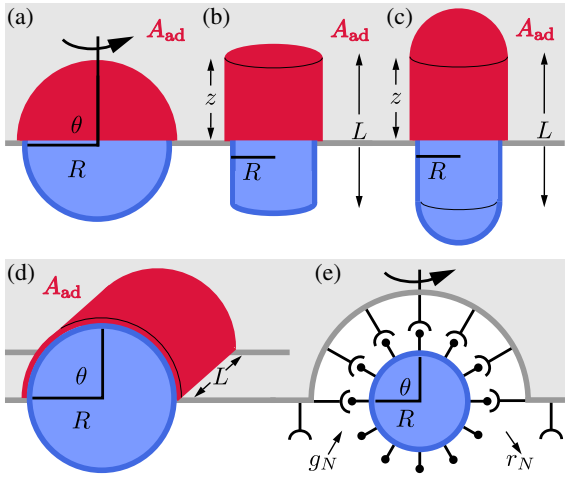

FIG. 1. Uptake of a particle of (a) spherical, (b) normal cylindrical (rocket mode), (c) spherocylindrical, and (d) parallel cylindrical shape (submarine mode). In a deterministic model, the virus is homogeneously covered with ligands adhering to the cell membrane along the adhesive area A_{ad}. (e) Stochastic uptake of a virus, for which the surface presents discrete ligands. The virus particle binds (unbinds) with a forward rate g_N (backward rate r_N) to receptors on the cell membrane.

receptor-mediated uptake is the role of particle shape [16,18,19]. More detailed approaches include the variational problem for finding minimal energy shapes [20,21], the role of receptor diffusion towards the nanoparticle [22,23], particle deformability [24,25], the physics of the scission step [26], and the role of the cytoskeleton [11]. In order to develop a stochastic description, here, we start with a minimal deterministic model, which we then extend to the stochastic case.

We assume that ligands to the cellular adhesive receptors are homogeneously distributed on the viral surface. The total free energy can be written as [27]

$$E_{\text{total}} = -\int_{A_{\text{ad}}} W dA + \int_{A_{\text{mem}}} 2\kappa H^2 dA + \sigma \Delta A, \quad (1)$$

where W is the adhesion energy per area, κ is the bending rigidity, H is the mean curvature, σ is the membrane tension, and ΔA the excess area due to the deformation (compared to the flat case). Typical parameter values are $W = 10^{-1}$ mJ/m^2, $\kappa = 25 k_B T$, and $\sigma = 10^{-4}$ N/m [28,29]. For example, a reovirus has 12 major and 60 minor ligands [12,30]. With a binding energy of around $15 k_B T$ each, one estimates $W = 4.4 \times 10^{-2}$ mJ/m^2 for a homogeneous adhesion model.

The two membrane parameters define a typical length scale of $\lambda = \sqrt{\kappa/\sigma} \approx 32$ nm. As shown schematically in Fig. 1, we consider a spherical or cylindrical particle of radius R adhering to the membrane. Then, the bending energy in Eq. (1) has contributions both from the adhering (A_{ad}) and free parts ($A_{\text{mem}} - A_{\text{ad}}$) of the membrane. It has been previously shown [18,28,29,31] that the contributions from the free part can be neglected in two special regimes. In the loose regime ($R \ll \lambda$), the free membrane can adopt the shape of a minimal surface, and thus its bending contribution vanishes. In the tense regime ($R \gg \lambda$), the free part is essentially flat, and the contribution from the adhered membrane is much larger than the one from the free membrane. To arrive at an analytical model, here, we neglect the contributions from the free membrane also for the intermediate case.

Equation (1) can now easily be analyzed for the geometries sketched in Fig. 1, namely, for a sphere ($\circ$) [Fig. 1(a)], for a cylinder oriented normally to the membrane ($\perp$) [Fig. 1(b)], for a spherocylinder ($\cap$) [Fig. 1(c)], and for a cylinder oriented parallel to the membrane ($\parallel$) [Fig. 1(d)]. Although it has been shown in coarse-grained molecular dynamics simulations that spherocylinders might undergo a dynamical sequence of first lying down and then standing up [16], the two cylindrical modes considered here are the paradigmatic configurations encountered during wrapping [18]. In the case of the normal cylinder, the top and bottom surfaces are neglected because they do not contribute to the uptake force. To keep our calculations as transparent as possible, we neglect them also for the parallel cylinder. In both cases, we neglect the bending energies at the kinked edges.

The uptake forces F_{up} are calculated by taking the variation of the energy with respect to the opening angle θ or height z, respectively, and are balanced by the friction force they experience: $F_{\text{up}} = F_{\text{friction}}$ [21]. For a spherical particle, the membrane covered area is a spherical cap of radius R and opening angle θ, i.e., $A^{\circ}_{\text{ad}} = 2\pi R^2(1 - \cos\theta)$, cf. Fig. 1(a). The friction force is $F^{\circ}_{\text{friction}} = \eta 2\pi R \sin(\theta) R\dot{\theta}$, i.e., an effective membrane microviscosity of order $\eta = 1$ Pa s times the change of the membrane-covered particle surface. The resulting equation of motion reads

$$\dot{\theta} = \nu_{\text{up}} - \nu_\sigma(1 - \cos\theta), \quad (2)$$

with $\nu_w = W/(R\eta)$, $\nu_\kappa = 2\kappa/(R^3\eta)$, $\nu_\sigma = \sigma/(R\eta)$, and $\nu_{\text{up}} = \nu_w - \nu_\kappa$. The uptake time can be calculated as [32]

$$T^{\circ}_{\text{det}} \approx \frac{\pi}{\nu_{\text{up}}\sqrt{1 - \frac{2\nu_\sigma}{\nu_{\text{up}}}}}. \quad (3)$$

Note that it diverges for $\nu_{\text{up}} = 2\nu_\sigma$, defining a critical radius R_{crit}, below which uptake is not possible. In the limit of vanishing σ, we recover the classical result $R_{\text{crit}} = \sqrt{2\kappa/W} \approx 44$ nm [17]. We note that our theory predicts normal uptake forces of around 10 pN, which agrees well with results from recent atomic force microscopy experiments [33,34].

Analogous calculations can be performed for the three cases with cylinders at equal volumes [32]. Figure 2(a) compares the resulting uptake times. For the normal and parallel cylinders, we take the same radius as for the sphere and adjust the aspect ratio. For the spherocylinder, we take the same aspect ratio as for the cylinders and adjust the radius. All four geometries show similar behaviors: a critical radius R_{crit} exists, below which uptake is not possible. The parallel cylinder has half the critical radius of the sphere because its mean curvature is half as large at equal radius. Moreover, an optimal radius R_* exists at which the uptake time is minimal [32]. Interestingly, the critical and optimal values are very close to each other, and the cylindrical particles are taken up faster than the spherical ones. The spherocylinder is the slowest case because, at equal volumes, the aspect ratio is modest and the spherical part dominates. Figures 2(b) and 2(c) display the uptake time for a spherical particle as a function of W and R or σ, respectively, showing that a smaller adhesion energy has to be compensated for by either a larger radius or smaller membrane tension. Importantly, in the deterministic case, certain parameter values do not lead to any uptake.

We now turn to the stochastic variant of our uptake model [cf. Fig. 1(e)]. For the sphere, we map the membrane-covered area onto the number of bound receptors N

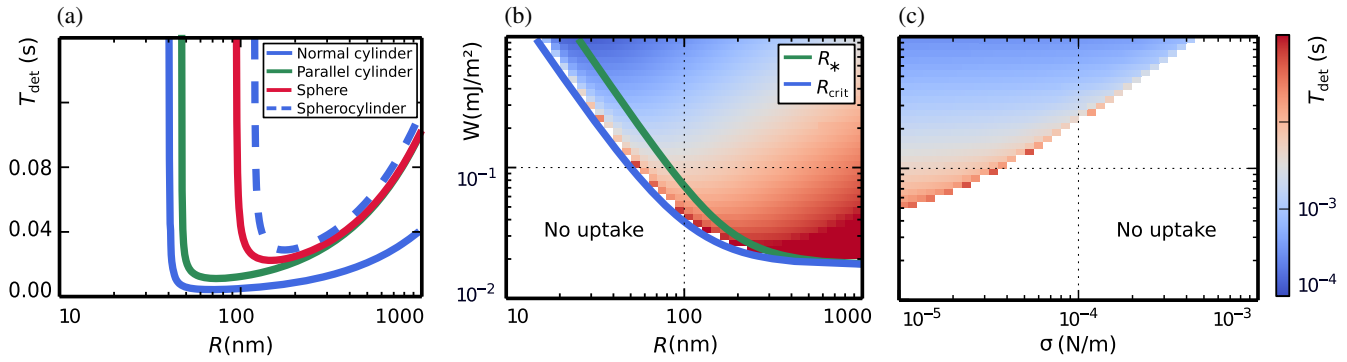

FIG. 2. Deterministic uptake dynamics. (a) Uptake times for sphere (red), normal cylinder (blue), spherocylinder (dashed blue), and parallel cylinder (green) as functions of radius R at equal particle volume. (b) and (c) Uptake times for a sphere as a function of adhesion energy W and radius R or membrane tension σ, respectively. In Fig. 2(b), the critical (optimal) radius for spherical uptake is shown in blue (green). Parameter values (if not varied) are $R = 90$ nm, $W = 4.4 \times 10^{-2}$ mJ/m^2, and $\sigma = 0.9 \times 10^{-5}$ N/m.

[32], assuming axial symmetry. Using Eq. (2), we find a dynamical equation for N through $\dot{N} = (dN/d\theta)\dot{\theta}$. From this discrete equation, a one-step master equation [35] can then be deduced, with the forward rate of $g_N = \nu_w N_{\mathcal{E}}$ and the backward rate of $r_N = \nu_\kappa N_{\mathcal{E}} + 2\nu_\sigma N_{\mathcal{E}}(N-1)/(N_{\max}-1)$, where $N_{\mathcal{E}}(N) = \sqrt{(N-1)[(N_{\max}-1)-(N-1)]}$ corresponds to the number of receptors at the advancing edge.

We first solved the master equation numerically using the Gillespie algorithm [36] and averaging over 10^4 trajectories. Figure 3(a) shows the resulting distribution of uptake times and the results for the number of bound receptors as a function of time (inset). Clearly, the mean uptake time is substantially smaller than the uptake time from the deterministic approach. Figures 3(b) and 3(c) display the simulated mean uptake times as a function of W and R or σ, respectively. When comparing to the deterministic approach, cf. Figs. 2(b) and 2(c), we see that, now, uptake is possible for any parameter value, although it can be rather long in regions where the deterministic model does not allow for uptake. However, the parameter region with uptake in experimentally accessible uptake times is strongly increased and now extends below the blue line, indicating the critical radius R_{crit} of the deterministic model. This expansion of the parameter regime that allows the process to complete is also known from the stochastic dynamics of small adhesion clusters [13,14].

We next discuss the interplay between the shape and stochastic dynamics in analytical detail. For simplicity, we set the membrane tension to zero in the following ($\sigma = 0$). We approximate the master equation by a Fokker-Planck equation (FPE) using a Kramers-Moyal expansion [35]. The equivalent stochastic differential equation can be transformed to angle space using Itô's lemma [37]

$$\dot{\theta} = \nu_{\text{up}} - D\frac{\cos\theta}{\sin^2\theta} + \sqrt{\frac{2D}{\sin\theta}}\xi(t), \tag{4}$$

where $D = (\nu_w + \nu_\kappa)/(N_{\max}-1)$. The noise $\xi(t)$ is assumed to be Gaussian with $\langle\xi(t)\rangle = 0$ and

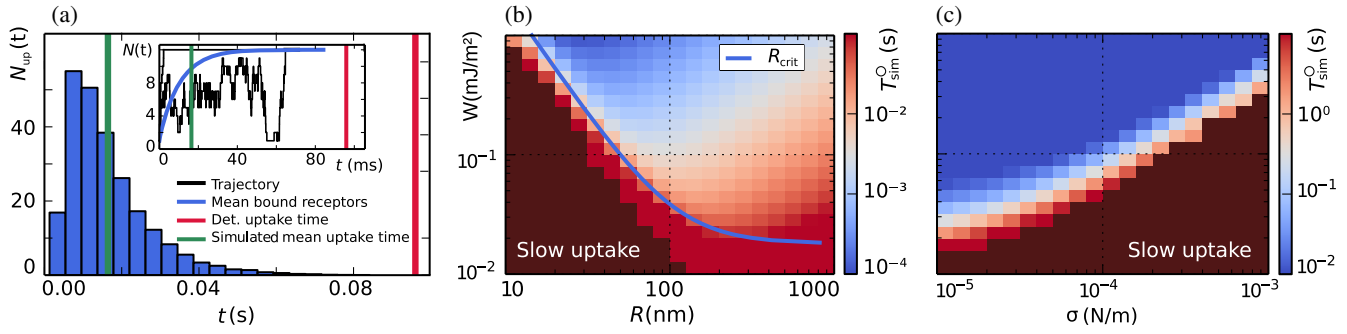

FIG. 3. Stochastic uptake dynamics for a spherical particle (reovirus with $N_{\max} = 12$). (a) Histogram of uptake times with obtained mean $T^{\circ}_{\text{sim}} \approx 16$ ms (green line; standard deviation is ≈11 ms) as compared to the deterministic value $T^{\circ}_{\text{det}} \approx 96$ ms (red line). (Inset) Two example trajectories (black) of the number of bound receptors as a function of time and the mean number $\langle N^{\text{sim}}\rangle$ obtained from simulating the master equation (blue). (b) and (c) Mean uptake time T°_{sim} as a function of W and either R or σ. In the dark colored region, uptake may still occur beyond the used simulation time. In Fig. 2(b), the blue line is the critical radius R_{crit} of the deterministic model. Parameter values are as in Fig. 2.

$\langle \xi(t)\xi(t')\rangle = \delta(t-t')$. From Eq. (4), one can directly read the drift term (or the corresponding potential) of the corresponding FPE in angle space and its diffusion coefficient D [32]. Because, for the spherical case, this diffusion constant depends on the state variable θ, here, we deal with multiplicative noise.

In marked contrast, for the two cylindrical cases, one obtains additive noise. For example, for the parallel cylinder, we find $\dot{\theta}^{\parallel} = \nu_{\mathrm{up}}^{\parallel} + \sqrt{2D^{\parallel}}\xi(t)$, where $\nu_{\mathrm{up}}^{\parallel} = W/(\eta R) - \kappa/(2R^3\eta)$ and $D^{\parallel} = (\nu_{\mathrm{up}}^{\parallel} + \kappa/(R^3\eta))\pi/(2(N_{\max}-1))$, where the latter does not depend on θ because the length of the moving contact line is constant [32]. The different quality of the noise suggests that the uptake dynamics change in a fundamental manner in the different geometries.

The mean uptake times can be obtained analytically by studying the mean first passage time problem using the backwards FPE [37,38] with a reflecting (adsorbing) boundary condition at $\theta = 0$ ($\theta = \pi$). Neglecting the angle dependent drift term (because it is large only for the first and last steps) but keeping the multiplicative noise, the mean uptake time evaluates to [32]

$$T_{\mathrm{mult}}^{\circ} = T_{\mathrm{det}}^{\circ}\left[1 - e^{-(\nu_{\mathrm{up}}/D)} I_0\left(\frac{\nu_{\mathrm{up}}}{D}\right)\right] < T_{\mathrm{det}}^{\circ}, \qquad (5)$$

where I_0 is the modified Bessel function of the first kind. In the limit of small fluctuations compared to the uptake frequency, we recover the deterministic limit. In the opposite limit of large fluctuations, the uptake time approaches $T_{\mathrm{mult}}^{\circ} \approx \pi/D$.

For the parallel cylinder, the noise is additive and the mean uptake time is readily obtained as [32]

$$T_{\mathrm{add}}^{\parallel} = T_{\mathrm{det}}^{\parallel} - \frac{D^{\parallel}}{\nu_{\mathrm{up}}^{\parallel 2}}\left[1 - \exp\left(-\frac{\pi\nu_{\mathrm{up}}^{\parallel}}{D^{\parallel}}\right)\right] < T_{\mathrm{det}}^{\parallel}, \qquad (6)$$

where $T_{\mathrm{det}}^{\parallel} = \pi/\nu_{\mathrm{up}}^{\parallel}$. In the limit of small fluctuations, one again recovers the deterministic uptake time, whereas for large fluctuations, one finds $T_{\mathrm{add}}^{\parallel} \approx \pi^2/(2D^{\parallel})$. Hence, for both geometries, the mean uptake time is always smaller than the deterministic one. In general, fluctuations in small systems combined with a reflecting boundary should always decrease the mean first passage time because the stochastic process profits from the presence of the boundary, whereas the deterministic process does not.

We now consider a particle with $R = 180$ nm, i.e., in the region of Fig. 2(a), in which the deterministic uptake times of the sphere and the parallel cylinder are similar. Figure 4(a) shows the mean uptake times for different geometries at equal volume as a function of the number of receptors. We note that, for the parallel cylinder, it is also possible to compute the uptake time directly from the master equation $T_{\mathrm{ana}}^{\parallel}$ [37]. The agreement between simulations (symbols) and analytical results (lines) is very good for cylinders and rather good for spheres. For a small number of receptors (i.e., strong fluctuations), the uptake of a sphere is faster than the one of a cylinder. We conclude that the uptake of spherical particles dynamically benefits from the noise. In fact, using, in Eq. (6), ν_{up} and D instead of $\nu_{\mathrm{up}}^{\parallel}$ and $D^{\parallel}$, we find that $T_{\mathrm{mult}}^{\circ} < T_{\mathrm{add}}^{\circ} < T_{\mathrm{det}}^{\circ}$ always holds.

Although membrane tension could not be treated analytically, it can be included in the simulations, and we get the same results: i.e., the uptake times are reduced by increasing stochasticity. Figure 4(b) shows the mean uptake times as a function of the dimensionless parameter $\alpha = \nu_\sigma/\nu_{\mathrm{up}}$ for different $N_{\max}$ and $R = 90$ nm. Although stochasticity is most important for small numbers of receptors, nevertheless, even for substantial numbers on

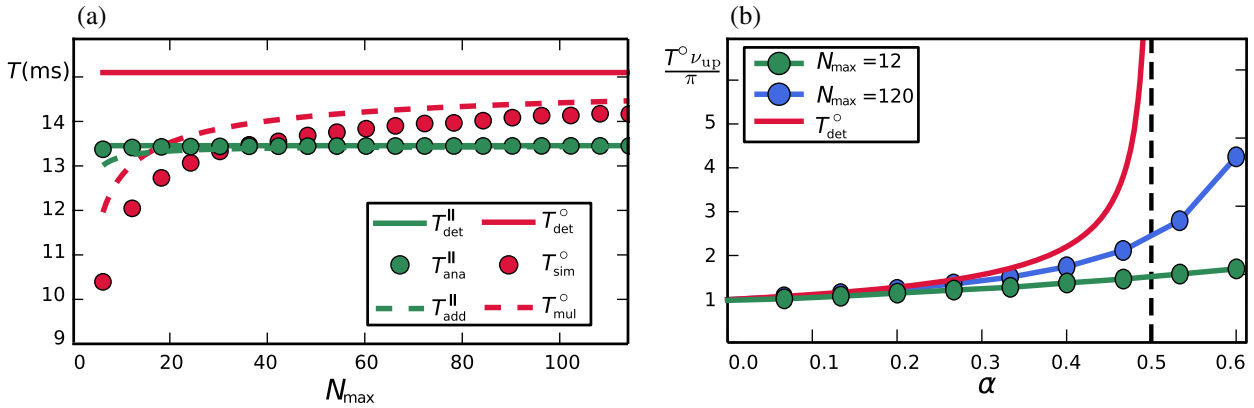

FIG. 4. (a) Geometry-dependent mean uptake times for spheres (red) and parallel cylinders (green) as a function of the maximum number of receptors. Shown are the analytical results for the deterministic case (solid) and for multiplicative (additive) noise corresponding to the spherical (cylindrical) geometry (dashed). The results from the simulations of the master equation are shown for the sphere (cylinder) as symbols. (b) The case with membrane tension can be treated with computer simulations. Shown are the mean uptake times for a sphere as a function of the dimensionless parameter $\alpha = \nu_\sigma/\nu_{\mathrm{up}}$ (by varying σ) for two different numbers of receptors and the deterministic case (diverging at $\alpha = 1/2$).

the order of one hundred receptors, the stochastic effects survive.

In conclusion, we found that the uptake of spherical particles profits from the presence of noise. Our results suggest yet another advantage for viruses to be spherical. Similar effects arising from the interplay of stochastic dynamics and geometry might also exist for other biologically relevant first passage problems, e.g., phagocytosis [39], the closure of transient pores on spherical vesicles [40], or the fusion of tissue over circular holes [41].

F. F. acknowledges support by the Heidelberg Graduate School for Fundamental Physics. The authors thank Steeve Boulant, Ada Cavalcanti-Adam, and Tina Wiegand for helpful discussions on reovirus, and we acknowledge the Collaborative Research Centre 1129 for support. U.S.S. acknowledges support as a member of the Interdisciplinary Center for Scientific Computing and the cluster of excellence CellNetworks.

[1] B. Alberts, *Molecular Biology of the Cell* (Garland Science, New York, 2015), 6th ed.
[2] D. S. Dimitrov, Nat. Rev. Microbiol. **2**, 109 (2004).
[3] S. Zhang, H. Gao, and G. Bao, ACS Nano **9**, 8655 (2015).
[4] J. Panyam and V. Labhasetwar, Adv. Drug Delivery Rev. **55**, 329 (2003).
[5] N. von Moos, P. Burkhardt-Holm, and A. Köhler, Environ. Sci. Technol. **46**, 11327 (2012).
[6] C. Hulo, E. De Castro, P. Masson, L. Bougueleret, A. Bairoch, I. Xenarios, and P. Le Mercier, Nucleic Acids Res. **39**, D576 (2011).
[7] F. H. Crick and J. D. Watson, Nature (London) **177**, 473 (1956).
[8] W. Roos, R. Bruinsma, and G. Wuite, Nat. Phys. **6**, 733 (2010).
[9] R. Zandi, D. Reguera, R. F. Bruinsma, W. M. Gelbart, and J. Rudnick, Proc. Natl. Acad. Sci. U.S.A. **101**, 15556 (2004).
[10] P. Kumberger, F. Frey, U. S. Schwarz, and F. Graw, FEBS Lett. **590**, 1972 (2016).
[11] S. X. Sun and D. Wirtz, Biophys. J. **90**, L10 (2006).
[12] E. S. Barton, J. C. Forrest, J. L. Connolly, J. D. Chappell, Y. Liu, F. J. Schnell, A. Nusrat, C. A. Parkos, and T. S. Dermody, Cell **104**, 441 (2001).
[13] T. Erdmann and U. S. Schwarz, Phys. Rev. Lett. **92**, 108102 (2004).
[14] T. Robin, I. M. Sokolov, and M. Urbakh, Phys. A **507**, 398 (2018).
[15] R. Vácha, F. J. Martinez-Veracoechea, and D. Frenkel, Nano Lett. **11**, 5391 (2011).
[16] C. Huang, Y. Zhang, H. Yuan, H. Gao, and S. Zhang, Nano Lett. **13**, 4546 (2013).
[17] R. Lipowsky and H.-G. Döbereiner, Europhys. Lett. **43**, 219 (1998).
[18] S. Dasgupta, T. Auth, and G. Gompper, Nano Lett. **14**, 687 (2014).
[19] A. H. Bahrami, M. Raatz, J. Agudo-Canalejo, R. Michel, E. M. Curtis, C. K. Hall, M. Gradzielski, R. Lipowsky, and T. R. Weikl, Adv. Colloid Interface Sci. **208**, 214 (2014).
[20] M. Deserno, Phys. Rev. E **69**, 031903 (2004).
[21] J. Agudo-Canalejo and R. Lipowsky, ACS Nano **9**, 3704 (2015).
[22] H. Gao, W. Shi, and L. B. Freund, Proc. Natl. Acad. Sci. U.S.A. **102**, 9469 (2005).
[23] P. Decuzzi and M. Ferrari, Biomaterials **28**, 2915 (2007).
[24] X. Yi, X. Shi, and H. Gao, Phys. Rev. Lett. **107**, 098101 (2011).
[25] C. Zeng, M. Hernando-Pérez, B. Dragnea, X. Ma, P. van Der Schoot, and R. Zandi, Phys. Rev. Lett. **119**, 038102 (2017).
[26] Z. A. McDargh, P. Vázquez-Montejo, J. Guven, and M. Deserno, Biophys. J. **111**, 2470 (2016).
[27] W. Helfrich, Z. Naturforsch. C **28**, 693 (1973).
[28] L. Foret, Eur. Phys. J. E **37**, 42 (2014).
[29] G. Kumar and A. Sain, Phys. Rev. E **94**, 062404 (2016).
[30] D. Veesler, K. Cupelli, M. Burger, P. Gräber, T. Stehle, and J. E. Johnson, Proc. Natl. Acad. Sci. U.S.A. **111**, 8815 (2014).
[31] M. Sadeghi, T. R. Weikl, and F. Noé, J. Chem. Phys. **148**, 044901 (2018).
[32] See Supplemental Material at http://link.aps.org/supplemental/10.1103/PhysRevLett.122.088102, which includes details on the deterministic and stochastic calculations, as well as three additional figures.
[33] D. Alsteens, R. Newton, R. Schubert, D. Martinez-Martin, M. Delguste, B. Roska, and D. J. Müller, Nat. Nanotechnol. **12**, 177 (2017).
[34] Y. Pan, F. Zhang, L. Zhang, S. Liu, M. Cai, Y. Shan, X. Wang, H. Wang, and H. Wang, Adv. Sci. Lett. **4**, 1600489 (2017).
[35] N. G. Van Kampen, *Stochastic Processes in Physics and Chemistry* (Elsevier, North-Holland, Amsterdam, 1984).
[36] D. T. Gillespie, J. Phys. Chem. **81**, 2340 (1977).
[37] C. W. Gardiner, *Handbook of Stochastic Methods* (Springer, Berlin Heidelberg New York, 1985).
[38] S. Redner, *A Guide to First-Passage Processes* (Cambridge University Press, Cambridge, England, 2001).
[39] S. Tollis, A. E. Dart, G. Tzircotis, and R. G. Endres, BMC Syst. Biol. **4**, 149 (2010).
[40] O. Sandre, L. Moreaux, and F. Brochard-Wyart, Proc. Natl. Acad. Sci. U.S.A. **96**, 10591 (1999).
[41] V. Nier, M. Deforet, G. Duclos, H. G. Yevick, O. Cochet-Escartin, P. Marcq, and P. Silberzan, Proc. Natl. Acad. Sci. U.S.A. **112**, 9546 (2015).